THE EFFECT OF THE MAGNETIZING INDUCTANCE ON THE SMALL-SIGNAL DYNAMICS OF THE ISOLATED CUK CONVERTER

Vatché Vorpérian

Jet Propulsion Laboratory

California Institute of Technology

Pasadena, California 91109

Abstract

The magnetizing inductance of the isolated Cuk converter introduces an undesirable pair of closely spaced complex zeros and poles, or a glitch, in the control-to-output transfer function. Limited analysis and experimentation in the past have shown that sufficient increase in the magnetizing inductance significantly reduces the glitch. In this work, the isolated Cuk converter with coupled input and output inductors has been studied and the dependence of the glitch on various circuit parameters has been determined analytically. A condition has been derived for the ratio of the capacitances of the two energy transfer capacitors which completely eliminates the glitch at a given operating point. With this condition satisfied, it is shown that the energy transfer capacitors can be easily damped by a simple RC network to eliminate the glitch for a range of operation about an operating point.

INTRODUCTION

The advent of power MOSFETs and magnetic materials has led to improvements in the efficiency and power density of PWM converters. For instance, it has been demonstrated that a 5V, 20A output isolated Cuk converter, switching at 100kHz, has an efficiency greater than 90% and a power density of 5 0W/in^3. Other PWM converters have demonstrated high efficiencies as reported in []]. Although the dynamics of the non-isolated basic Cuk converter have been analyzed in detail [2], some problems associated with its isolated and coupled-inductor variations have riot, been addressed thoroughly. It has long been known that the magnetizing inductance of the isolation transformer in the Cuk converter introduces an undesirable glitch in the control-to-output transfer function which up until now has received limited attention and analysis [4] and [5]. The purpose of this paper is to provide a detailed analytical study of this effect and provide a simple remedy.

Since the isolated Cuk converter with coupled inductors is a sixtli-order system, the easiest way to analyze it is to use tile model of the PWM switch as described in [6], [7] and [8]. The model of the PWM switch also has the added advantage that it allows for the converter model to be easily implemented on a circuit simulation programs such as Pspice [9].

THE CONTROL-TO OUTPUT TRANSFER FUNCTION

The isolated Cuk converter with its input and output inductors coupled is shown in Fig. 1a. All the elements are reflected to the primary side as shown in Fig. 1b and the PWM switch is identified and shown explicitly in Fig. 1c. For the reflected elements we have:

$$C'_2 = C'_{2s}/N^2 \tag{1a}$$

$$C'_o = C'_{os}/N^2 \tag{1c}$$

$$L_2 = L_{2s}N^2 \tag{1b}$$

$$R = R_{L}N^2 \tag{1d}$$

$$N = N_p/N_s \tag{1e}$$

The coupling coefficient k, is the same in the reflected and the original circuit. The coupled inductors are replaced with their equivalent circuit model in which

$$l_a = L_1(1 - k^2) \tag{2a}$$

$$L_M = L_1 k^2 \tag{2b}$$

$$n = \frac{1}{k}\sqrt{L_2/L_1} \tag{2c}$$

Since continuous conduction is the dominant mode of operation, the converter will be analyzed in continuous conduction mode (CCM). (If synchronous rectification is used, then CCM is the *only* mode of operation.) As explained in [6], the *only* step required to arrive from the original converter circuit to its small-signal equivalent circuit is to replace the PWM switch with its equivalent circuit model in CCM as shown in Fig. 2. With a small-signal equivalent circuit model of the power converter, one can perform design-oriented analysis and obtain low-entropy expressions [3]. As usual, the quiescent, or the dc operating point is determined first as shown in Fig. 3a in which all the reactive elements and the perturbation sources are set to zero. A dc analysis of the circuit in Fig. 3a yields:

$$M \equiv \frac{V_o}{V_g} = -\frac{D}{D'} \tag{3a}$$

$$V_{ap} = -V_g/D' \tag{3b}$$

$$I_c = -\frac{V_g \ D}{R \ D'^2} \tag{3c}$$

(If all the parasitic elements are included as shown in Fig 3b, a dc analysis of the conversion ratio yields:

$$M = \frac{D}{D'} \, \eta$$

in which η is the average conversion efficiency given by

$$\eta = \frac{1}{1 + \frac{r_{L_2}}{R} + \left(\frac{D}{D'}\right)^2 r_{L_1} + \frac{r_e}{R} \frac{1}{D'^2}}$$

where

$$r_e = DD'(r_{C_1} + r_{C_2} + r_{pw} + r_{sw}) + Dr_t + D'r_d$$

$r_{C_1} \equiv$ Equivalent series resistance of C_1

$r_{C_2} \equiv$ Equivalent resistance of C_2 reflected to primary

$r_{pw} \equiv$ Resistance of primary winding

$r_{sw} \equiv$ Resistance of secondary winding reflected to primary

$r_t \equiv$ On-Resistance of the active MOSFET switch

$r_d \equiv$ On-Resistance of the passive MOSFET switch (synchronous rectifier) reflected to the primary

In carrying out the small-signal analysis, the parasitic elements will be ignored at first but will be included later to determine their effect on the high-Q glitch. The corrections on the dc operating point of the PWM switch in the presence of parasitic elements are given in detail in [6] and have no significant effect on the small-signal characteristics.)

The control-to-output transfer function is given by

$$G_d(s) \equiv \frac{\hat{v}_o(s)}{\hat{d}(s)} = K_d \frac{N(s)}{D(s)} \tag{4}$$

in which each of K_d, $N(s)$ and $D(s)$ will be determined separately. The derivative of the output voltage with respect to the duty ratio gives K_d

$$K_d = \frac{d}{dD} V_o = \frac{V_o}{DD'} \tag{5}$$

The numerator $N(s)$ is determined by studying the null condition in $\hat{i}_{L_2}(s) = 0$ shown in Fig. 4a which reduces the circuit to the one in Fig. 4b. By application of an extension of the extra-element theorem [10] and [11] to N extra elements, the numerator is determined to be given by

$$N(s) = 1 + \sum_{n=1}^{n=4} a_n s^n \tag{6}$$

$$a_1 = \frac{L_1}{R}\left(a + \frac{D}{D'}\right)\frac{D}{D'}$$ (7a)

$$a_2 = L_1\left(C_1 + a\frac{D}{D'}C_2\right) + L_m(C_1 + C_2)$$ (7b)

$$a_3 = -\frac{L_1}{R}L_m(C_1 + C_2)\left(a + \frac{D}{D'}\right)\frac{D}{D'}$$ (7c)

$$a_4 = L_1 L_m C_1 C_2, \frac{a + \frac{D}{D'}}{1 - a} + D$$ (7d)

where

$$a = \frac{L_M}{L_M + L_\sigma}, \quad n = k\sqrt{L_2/L_1}$$ (8)

Using the same theorem, the denominator $D(s$ is determined from the circuit in Fig. 5 in which all the excitation sources are set to zero. The denominator and its coefficients are given by:

$$D(s) = + \sum_{n=1}^{n=6} b_n s^n$$ (9)

$$b_1 = \frac{L_e}{R}$$ (10a)

$$b_2 = L_1 C_e \cdot L_m(C_1 + C_2) + L_e C_o$$ (10b)

$$b_3 = L_m(C_1 + C_2)\frac{L_e}{R} + L_2 C_e \frac{L_a}{R}$$ (10c)

$$b_4 = L_1 C_1 L_m \frac{C_2}{D'^2} + L_m(C_1 + C_2)C_a L_e + L_a C_2 L_2 C_o$$ (10d)

$$b_5 = \frac{L_2}{R}L_a C_1 L_m \frac{C_2}{D'^2}$$ (10e)

$$b_6 = L_2 C_o L_a C_1 L_m \frac{C_2}{D'^2}$$ (10f)

where

$$C_e = C_1 + C_2 \frac{D}{D'^2}$$

$$L_e = L_a\left(\frac{D}{D'}\right)^2 + L_M\left(n + \frac{D}{D'}\right)^2 = L_1\left(\frac{D}{D'}\right)^2 + L_2 + 2k\sqrt{L_1 L_2}$$ (12)

The component values used for the evaluation of this control-to-output transfer function are taken from a practical converter design example given in [5] and listed here in Table 1. The magnitude response is shown in Fig. 6 in which the high-Q resonant glitch occurs at $f = 670$Hz. It was acknowledged in [5] that it was rather hard to damp this resonance by damping the energy transfer capacitors and the only remedy proposed was to increase the magnetizing inductance. In the sequel, using certain approximations, the control-to-output transfer function obtained in this section will be factored analytically in order to isolate the complex poles and zeros of the glitch from the rest of the transfer function. From the analytical expression obtained, a condition will be derived for the elimination of the glitch at a particular operating point by placement of its complex poles and zeros on top of each other. The contribution of the parasitic elements will be accounted for analytically in order to obtain a realistic estimate of the high Q of the complex poles and zeros of the glitch. Finally, it will be shown that a small amount of parallel damping applied to the energy transfer capacitor of I the input side will completely eliminate the glitch from a wide range of operation.

DETERMINATION OF THE GLITCH AND A CONDITION FOR ITS REMOVAL

1 he position of the complex poles of the glitch

Apart from introducing the high-Q resonant glitch, the magnetizing inductance L_m has little effect on the rest of the shape of the control-to-output transfer function. Therefore, the dominant fourth-order behavior of the denominator is determined first by taking the limit $L_m \to \infty$ in $G_d(s)$ as follows

$$\lim_{L_m \to \infty} G_d(s) = A \frac{N_\infty(s)}{D_\infty(s)} \tag{13}$$

where

$$D_\infty(s) = 1 + \sum_{n=1}^{n=3} b_n' s^n \tag{14}$$

where

$$b_1' = \frac{L_e}{R} \tag{15a}$$

$$b_2' = L_1 \frac{C_1 \| C_2}{D'^2} + C_o L_e \tag{15b}$$

$$b_3' = \frac{L_2}{R} L_\sigma \frac{C_1 \| C_2}{D'^2} \tag{15c}$$

$$b_4' = L_2 C_o L_\sigma \frac{C_1 \| C_2}{D'^2} = b_3'(C_o R) \tag{15c}$$

For a properly designed converter operating in CCk'l, the low and high frequency quadratic components are well separated, so that $D_\infty(s)$ factors approximately as follows:

$$D_\infty(s) \sim (1 + b_1's + b_2's^2)(1 + \frac{b_3'}{b_2'}s + \frac{b_4'}{b_2'}s^2) \tag{16a}$$

which can be written as

$$D_\infty(s) \sim \left(1 + s/Q_L\omega_L + (s/\omega_L)^2\right)\left(1 + s/Q_H'\omega_H' + (s/\omega_H')^2\right) \tag{16b}$$

where

$$\omega_L = \frac{1}{\sqrt{b_2'}} = \frac{1}{\sqrt{L_1 \frac{C_1 \| C_2}{D'^2} + C_o L_e}} \tag{17a}$$

$$Q_L = \frac{R}{\omega_L L_e} \tag{17b}$$

$$\omega_H' = \sqrt{\frac{b_2'}{b_4'}} = \sqrt{\frac{L_1}{L_2 L_\sigma C_o} + \frac{L_e}{L_2 L_\sigma} \frac{D'^2}{C_1 \| C_2}}$$

$$= \sqrt{\frac{1}{L_1 C_1 \| C_2} \frac{(D' + D/n)^2}{1 - k^2} + \frac{1}{L_2}\left(\frac{D^2}{C_1 \| C_2} + \frac{1}{C_o(1 - k^2)}\right)} \tag{18a}$$

$$Q_H' = \frac{1}{\omega_H'} \frac{b_2'}{b_3'} = \frac{C_o R}{\omega_H'} \frac{b_2'}{b_4'} = \omega_H' C_o R \tag{18b}$$

The numerator is given by

$$N_\infty(s) = 1 + a_1's + a_2's^2 \tag{20}$$

$$a_1' = -\frac{L_1}{R}\left(\alpha + \frac{D}{D'}\right)\frac{D}{D'} \tag{21a}$$

$$a_2' = L_1 C_1 \| C_2 \frac{\alpha + \frac{D}{D'}}{\frac{\alpha}{1 - \alpha} + D} \tag{21b}$$

At this point only ω_L and Q_L are of interest to us because the high frequency quadratic will be determined later again. $N_\infty(s)$, ω_H' and Q_H' are given for completeness, because these factors, to the best of the author's knowledge, have not been derived before for the nonisolated Cuk converter with coupled inductors. (Note that in the limit $L_m \to \infty$ the energy transfer capacitors, C_1 and C_2 become connected in series and act as a single energy transfer capacitor with an equivalent value $C_1 \| C_2$ in the

nonisolated Cuk converter. A l s o , note that in the limit $k \to 1$ the high frequency corner moves to infinity, $\omega'_H \to \infty$, and the order of the system is reduced by two, i.e., $D_\infty(s)$ becomes a second-order polynomial.)

Two cases of the relative position of the glitch with respect to the high-frequency corner, ω_H, will be considered. The case in which the glitch occurs above the high-frequency corner is not as practical and will be discussed later in the Appendix. In the more practical case, the glitch occurs below the high frequency corner

$$\omega_G < \omega_H \tag{22}$$

so that $D(s)$ can be factored approximately into two quadratic factors corresponding to the low-frequency and the glitch components respectively

$$D(s) \simeq \left(1 + s/Q_L\omega_L + (s/\omega_L)^2\right)\left(1 + s/Q_G\omega_G + (s/\omega_G)^2\right); \quad \omega_G < \omega_H \tag{23}$$

It is important to realize that no assumption has been made in (23) about the relative position of ω_G with respect to ω_L. In terms of the coefficients b_i, $D(s)$ can be written as

$$D(s) \simeq 1 + b_1 s + b_2 s^2 + b_3 s^3 + b_4 s^4 \tag{24}$$

Expansion of (23) and comparison with (24) yield

$$b_2 = \frac{1}{\omega_L^2} + \frac{1}{\omega_G^2} + \frac{1}{\omega_L\omega_G Q_L Q_G} \simeq \frac{1}{\omega_L^2} + \frac{1}{\omega_G^2} \tag{25}$$

The approximation in the last step in Eq. (25) is valid because the position of the resonances are hardly effected by the damping factors in a relatively high-Q system. Substitution for ω_L arid b_2 in Eq. (25) yields

$$\omega_G \simeq \frac{1}{\sqrt{L_1\left(C_c - \frac{C_1 \| C_2}{D'^2}\right) + L_m(C_1 + C_2)}} \tag{26}$$

Although at this point Q_G can be determined by comparing the cubic terms in Eqs. (24) and (23), the result would not be of any practical value because the parasitic resistances of C_1, C_2 and L_1 have a much stronger effect on Q_G. In the next section, Q_G will be determined in terms of these parasitic resistances.

For a properly designed converter the numerator can be factored into two well separated quadratics

$$N(s) = \left(1 + s/Q_g \omega_g + (s/\omega_g)^2\right)\left(1 + s/Q_h' \omega_h + (s/\omega_h)^2\right) \tag{27}$$

Expansion of Eq. (27) and comparison with the coefficients a_i in Eqs. (7a-d) yield

$$a_1 = \frac{1}{\omega_g Q_g} + \frac{1}{\omega_h Q_h'} \tag{28a}$$

$$a_2 = \frac{1}{\omega_g^2} + \frac{1}{\omega_h^2} + \frac{1}{\omega_g \omega_h Q_h' Q_g} = \frac{1}{\omega_g^2}\left(1 + \left(\frac{\omega_g}{\omega_h}\right)^2 + \frac{\omega_g}{\omega_h Q_h' Q_g}\right) \simeq \frac{1}{\omega_g^2} \tag{28b}$$

$$a_3 = \frac{1}{\omega_g^2} \frac{1}{\omega_h Q_h'}\left(1 + \frac{\omega_g}{\omega_h}\frac{Q_h'}{Q_g}\right) \simeq \frac{1}{\omega_g^2} \frac{1}{\omega_h Q_h'} \tag{28c}$$

$$a_4 = \frac{1}{\omega_h^2}\frac{1}{\omega_g^2} \tag{28d}$$

No approximation is possible in Eq. (28a) because $Q_g >> Q_h'$ and $\omega_h >> \omega_g$ and both terms are comparable. The frequency of the complex zero corresponding to the glitch is obtained from Eq. (28b)

$$\omega_g \simeq \frac{1}{\sqrt{a_2}} = \frac{1}{\sqrt{L_1\left(C_1 - \alpha C_2 \frac{D}{D'}\right) + L_m(C_1 + C_2)}} \tag{29}$$

In the next section, Q_g will be determined in the presence of parasitic elements in order to obtain a more realistic value for it. The high frequency quadratic and its damping are obtained from Eqs. (28d) and (28c) respectively

$$\omega_h \simeq \sqrt{\frac{\frac{\alpha}{1-\alpha} + D}{\alpha + \frac{D}{D'}}\left[\frac{1 - \alpha\frac{D}{D'}\frac{C_2}{C_1}}{L_m C_2} + \frac{1}{L_1 C_1 \| C_2}\right]} \tag{30a}$$

$$Q_h' = \frac{1}{\omega_h}\frac{a_2}{a_3} = \frac{R}{\omega_h L_1}\frac{1}{\left(\alpha + \frac{D}{D'}\right)\frac{D}{D'}}\left[\frac{L_1}{L_m}\frac{1 - \alpha\frac{D}{D'}\frac{C_2}{C_1}}{1 + \frac{C_2}{C_1}} + 1\right] \tag{30b}$$

In the next section Q_h will be determined in the presence of parasitic elements.

Condition for the removal of the glitch

It is apparent for Fig. 6 that the Q-factors of the complex zeros and poles of the glitch are high and comparable. Therefore, it may be possible 10 eliminate the glitch by placing its zeros and poles on top of each other. This requires that

$$\omega'_g = \omega_G \tag{31}$$

which gives

$$\frac{C_2}{C_1} = \frac{D'}{D}\left[\frac{1 + D(1 - \alpha)}{D + \alpha D'}\right] \tag{32}$$

Two important special cases of this condition are given by $\alpha = 1$ and $\alpha = 0$ which correspond to the cases of zero-ripple coupling and no coupling at all respectively

$$\frac{C_2}{C_1} = \begin{cases} D'/D) & \alpha = 1 \quad \text{zero-ri)))le coupling} \\ 1/D^2 - 1 & \alpha = 0 \quad \text{no coupling} \end{cases} \tag{33}$$

Note that when the first of the two conditions in Eq. (33) is satisfied $\omega_g = \omega_G = 1/\sqrt{L_m(C_1 + C_2)}$. For the converter example given in the previous section, the input and output inductors are coupled for zero ripple current in the output filter so that $\alpha = 1$. Hence, according to Eq. (33), we choose the value of C_2 such that

$$\frac{C_2}{C_1} = \frac{D'}{D} = \frac{.7}{.3} \Rightarrow C_2 = .77\mu F \text{ or } C_{2s} = 14.7\mu F$$

This requires that C_{2s} be reduced from $66\mu F$ to $14.7\mu F$ which hardly effects tile main performance of the converter since the two energy transfer capacitors "arc in series so that the smallest of the two dominates their combined effect. (For this converter, if we choose $C_{2s} = 66\mu F$, then we have $C_1 \| C_2 = .33 \| 3.51 = .3\mu F$ which is not that much different than $C_1 \| C_2 = .23\mu F$ for a better choice of $C_{2s} = 14.7\mu F$.) The control-to-output transfer with this condition satisfied is shown in Fig. 7 in which the glitch has entirely disappeared.

For values of D outside the one chosen for the cancellation condition, the glitch reappears. For example, if the converter is designed to operate from a nominal input voltage of 270V with ± 20% variation, then the doty ratio would have to vary in the range $.258 < D < .342$. In this case the glitch reappears as shown in Fig. 8a but the separation between the poles and zeros is much smaller than if

the cancellation condition is not satisfied as shown in Fig. 8b. In Fig. 8a the maximum separation is 29Hz with considerable peaking while in Fig. 8b the maximum separation is 8Hz with much less peaking. Hence, with the cancellation condition satisfied, it should be much easier to damp out the energy transfer capacitors **as** will be shown later.

It can also be seen form Eqs. (26) and (29) that if L_m is made larger, the poles and zeros of the glitch become more closely spaced. This fact was recognized in [5] by experimenting with larger values of L_m until the glitch became unnoticeable. For the practical converter example, it was found in [5] that increasing L_m from 15mH to 60mH was adequate for eliminating the glitch. A four times increase in the magnetizing inductance, however, required a redesign of the isolation transformer to accommodate twice the number of turns.

THE EFFECT OF PARASITIC ELEMENTS ON THE GLITCH

In order to give a complete analytical description of the glitch, expressions are derived for the damping of its high-Q poles and zeros.

The damping of the poles of the glitch

The presence of the dominant term $L_m(C_1 + C_2)$ in the expressions for the frequencies of the pole and zero of the glitch suggests that the quadratic factor of the glitch in the denominator is given by the parallel combination of L_m, C_1 and C_2 as shown in Fig. 9. When the parasitic elements are included, the denominator of this system is of third order and is given by

$$D(s) = 1 + s(C_1 r_1 + C_2 r_2) + s^2(C_1 r_1 + C_2 r_2 + L_m(C_1 + C_2))$$

$$+ s^3 C_1 C_2 L_m(r_1 + r_2) \tag{34}$$

in which

$$r_1 = r_{C_1} + r_{pw} \tag{35a}$$

$$r_2 = r_{C_2} + r_{sw} \tag{35b}$$

in which r_{pw} and r_{sw} are the primary and secondary resistance of the isolation transformer respectively. Since, the parasitic resistances are small, the system must essentially exhibit a high-Q second-order resonance at $1/\sqrt{L_m(C_1 + C_2)}$ so that $D(s)$ can be factored to an excellent approximation as

$$D(s) \simeq (1 + s/\omega_o Q_G + (s/\omega_o)^2)(1 + s/s_p) \tag{36}$$

By expanding Eq. (36) and comparing coefficients of powers of s in Eq. (34) we find

$$\frac{1}{\omega_o Q_G} + \frac{1}{s_p} = C_1 r_1 + C_2 r_2 \tag{37a}$$

$$\frac{1}{\omega_o^2} \simeq L_m(C_1 + C_2) \tag{37b}$$

$$\frac{1}{\omega_o^2 s_p} = C_1 C_2 L_m (r_1 + r_2) \tag{37c}$$

A simple substitution of Eqs. (37c) and (37b) in (37a) yields

$$Q_G = \frac{1}{\omega_G(C_1 r_1 + C_2 r_2 - C_1 \| C_2(r_1 + r_2))} \tag{38}$$

in which instead of ω_o, the more accurate value of ω_G is used. Q_G can also be expressed as

$$Q_G = Q_1 \| Q_2 \| Q_p \tag{39}$$

in which

$$Q_1 = \frac{1}{\omega_G C_1 r_1} \tag{40a}$$

$$Q_2 = \frac{1}{\omega_G C_2 r_2} \tag{40b}$$

$$Q_p = -\frac{1}{\omega_G C_1 \| C_2(r_1 + r_2)} \tag{40c}$$

7he **damping** *of the zeros of the glitch*

Determination of the damping of the zeros of the glitch is considerably more difficult and requires the redetermination of the coefficients a_1 and a_3 in the presence of the parasitic elements. These coefficients are given by

$$a_1 = r_{L_1} \frac{L_m}{R} \frac{D'}{a + D/D'} \frac{D'}{D} + C_1\left(r_1 + r_{L_1} \| (-RD'^2/D^2)\right) + C_2 r_2 \tag{41}$$

$$a_3 = L_1 C_1 C_2 \frac{r_1 - \frac{R}{\alpha + D/D'}\frac{D'}{D}}{r_{L_1} - \frac{R}{\alpha + D/D'}\frac{D'}{D}} \left[r_2 + \frac{R}{1 + \frac{D}{\alpha D'} - \frac{D'}{\alpha D}\frac{R}{r_1}} \right]$$

$$+ L_m C_1 C_2 \left(r_1 + r_{L_1} \| (- RD'^2/D^2) \right) \frac{r_2}{r_1 \| r_2} \cdot \frac{1 + r_{L_1}/(r_1 + r_2) \| (- RD'^2/D^2)}{1 + r_{L_1}/r_1 \| (- RD'^2/D^2)}$$

$$+ \frac{L_1 L_m (C_1 + C_2)}{r_{L_1} - \frac{R}{\alpha + D/D'}\frac{D'}{D}} \tag{42}$$

There is no need to redetermine the coefficients a_2 and a_4 because these correspond to the resonant frequencies which are hardly effected by the parasitic elements. Equations (41) and *(4'2)* can be readily simplified as

$$a_1 \simeq - \frac{L_1}{R}(\alpha + D/D')\frac{D}{D'} + C_1(r_1 + r_{L_1}) + C_2 r_2 \tag{43}$$

$$a_3 \simeq L_1 C_1 C_2 (r_2 - \alpha r_1 \mathbf{1})/\mathbf{1})')$$

$$+ L_m C_1 C_2 (r_1 + r_2 + r_{L_1}) \frac{L_1 L_m (C_1 + C_2)}{R}\left(\alpha + \frac{D}{D'}\right)\frac{D}{D'} \tag{44}$$

According to Eq. (28a), (28b) and (28c) we have

$$\frac{1}{\omega_g Q_g} = a_1 - \frac{1}{\omega_h Q_h} = a_1 - \frac{a_3}{a_2} \tag{45}$$

In this equation, when the first **two** terms of a_3, given in Eq. *(44)*, are divided by a_2 we approximate a_2 by $a_2 \simeq L_m(C_1 + C_2)$, but when the last term of a_3 is divided by a_2 we use the following slightly better approximation

$$\frac{1}{a_2} = \frac{1}{L_m(C_1 + C_2) + L_1(C_1 - \alpha C_2 D/D')} \simeq \frac{1}{L_m(C_1 + C_2)}\left[1 - \frac{L_1(C_1 - \alpha C_2 D/D')}{L_m(C_1 + C_2)}\right] \tag{46}$$

The reason for this is that the terms in a_1 and a_3 which depend entirely on the load R **will** not cancel out. Substituting Eqs. (43) and (44) in (45) and making use of the approximations of a_2 we get

$$Q_g = q_1 \| q_2 \| q_p \| q_R \tag{47}$$

in which

$$q_1 = \frac{1}{\omega_g C_1 (r_1 + r_{L_1})} \tag{48a}$$

$$q_2 = \frac{1}{\omega_g C_2 r_2} \tag{48b}$$

$$q_p = -\frac{1}{\omega_g C_1 \| C_2 \left[r_2(1 + L_1/L_m) + r'_1 (1 - \alpha D/D') + r_{L_1} \right]} \tag{48c}$$

$$q_R = -\frac{1}{\omega_g L_1} \left\{ \frac{L_m}{-L_1} \frac{C_1 - i C_2}{C_1 - C_2 \alpha D/D'} \right. \tag{48d}$$

This completes the determination of the frequency response of the glitch.

The Q-factor, Q'_h, of $N_h(s)$, given earlier in Eq. (30b), will now be redetermined in the presence of the parasitic elements

$$Q_h = -\frac{Q'_h}{1 - \frac{RC_1 \| C_2}{\left(\alpha + \frac{D}{D'} \right) \frac{D}{D'}} \left[2 - \frac{\alpha r_1 D/D'}{L_m} + \frac{r_1 + r_2 + r_{L_1}}{L_1} \right]} \tag{49}$$

7he complete control- to-output transfer function

The control-to-output transfer function can now be written as

$$G_d(s) = K_d \frac{N_h(s)}{D_L(s) D_H(s)} \frac{N_g(s)}{D_G(s)} \tag{50}$$

in which the glitch in the frequency response is given by the complex pair of poles and zeros given by

$$N_g(s) = 1 + s/Q_g \omega_g + (s/\omega_g)^2 \tag{51a}$$

$$D_G(s) = 1 + s/Q_G \omega_G + (s/\omega_G)^2 \tag{51b}$$

in which ω_G, ω_g, Q_G and Q_g are given by Eqs. (26), (29), (38) and (47) respectively. The remaining parts of the transfer function arc

$$N_h(s) = 1 + s/Q_h \omega_h + (s/\omega_h)^2 \tag{52}$$

$$D_L(s) = 1 + s/Q_L \omega_L + (s/\omega_L)^2 \tag{53}$$

$$D_H(s) = 1 + s/Q_H \omega_H + (s/\omega_H)^2 \tag{54}$$

in which ω_L, Q_L, ω_h and Q_h were determined earlier in Eqs. (17a), (17b), (30a) and (49) respectively. Next, we will determine ω_H and Q_H which are the improved approximations to ω'_H and Q'_H given earlier in Eqs. (18a) and (18b) respectively. Since $(\omega_L \omega_H \omega_G)^2 = 1/b_6$ we have

$$\omega_H = \frac{1}{\omega_G \omega_L \sqrt{b_6}} = \omega'_H \sqrt{1 + \frac{C_c - (C_1 \| C_2)/D'^2}{C_1 + C_2} \frac{L_1}{L_m}} \qquad (55)$$

When the conditions for the removal of the glitch and zero-ripple coupling (Eq. (33)) are satisfied, then

$$\alpha = 1 \text{ and } \frac{C_2}{C_1} = \frac{D'}{D} \Rightarrow \omega_H = \omega'_H = \sqrt{\frac{1}{L_2 C_o} \frac{1}{1 - k^2} + \frac{D^2 + (nD' + D)^2/(n-1)}{L_2 C_1 D'}} \qquad (56)$$

which is independent of L_m. As the duty ratio varies about the value satisfying the removal condition, ω_H acquires a small dependence on the magnetizing inductance L_m.

Since the primary focus of this section is the glitch, the dependence of Q_H on the parasitic elements will not be determined. A somewhat improved approximation for Q_H, however, can be obtained as follows:

$$Q_H = \frac{1}{\omega_H} \frac{b_4}{b_5}$$

$$= \frac{R}{\omega_H L_2} \left[\frac{1}{1 - k^2} + \frac{C_o}{C_1 \| C_2} \left[D^2 + \frac{(nD' + D)^2}{n-1} \right] + \frac{L_2}{L_m} \frac{C_o}{(C_2/D'^2) \| (C_1/D^2)} \right] \qquad (57a)$$

which can also be expressed in terms of Q'_H as

$$Q_H = \frac{Q'_H}{\sqrt{1 + \frac{C_c - (C_1 \| C_2)/D'^2}{C_1 + C_2} \frac{L_1}{L_m}}} + \frac{R}{\omega_H L_m} \frac{C_o}{\frac{C_2}{D'^2} \| \frac{C_1}{D^2}} \qquad (57b)$$

If the removal and zero-ripple coupling conditions are satisfied, then Q_H is given by

$$\alpha = 1 \text{ and } \frac{C_2}{C_1} = \frac{D'}{D} \Rightarrow Q_H = Q'_H + \frac{R}{\omega_H L_m} \frac{C_o D'}{C_2} \qquad (58)$$

The approximate and exact transfer functions for the practical converter discussed earlier are compared in Figs. 10 and 11 for $D = .342$. In Fig.10 all the circuit components are the same as those in Table 1 except that the energy transfer capacitor C_{2s} has been chosen to be $C_{2s} = 14.7\mu F$

$(C_2 = .77\mu F)$ to satisfy the removal condition at $D = .3$. Also, the following parasitic components have been added:

$$r_1 = .0\Omega \qquad r_2 = .5\Omega \qquad r_{1_1} = .01\Omega$$

In order to verify the validity of Q_G and Q_g derived in Eqs. (38) and (47), the region in the vicinity of the glitch is expanded in Fig. 11. It can be seen from both figures that the agreement between the approximate and exact transfer functions is very good. Since we have not accounted for the dependence of Q_H on the parasitic elements, there is a discrepancy in the peaking at ω_H between the approximate and the circuit models. The frequencies and the Q-factors of the poles and zeros of the glitch for this example were computed to be

$$f_g = 1245 Hz \qquad Q_g = 254 \tag{59a}$$
$$f_G = 1252 Hz \qquad Q_G = 400 \tag{59b}$$
$$\Delta f = f_g - f_G = 7 Hz \tag{59c}$$

It is important to see that although the Q-factors of the glitch are high, the magnitude of the transfer function at the peaks is only 10 to 13 decibels away from the smooth curve. Of course the reason for this is that ω_g and ω_G are closely spaced. Hence, the glitch can be nearly eliminated if the Q-factors are reduced by a factor of 0 which can be easily accomplished by tightly damping the energy transfer capacitor C_1 as will be shown in the next section. The amount by which the magnitude of the transfer function peaks at ω_g and ω_G can be easily determined by evaluating the magnitude of $N_g(s)/D_G(s)$ at ω_g and ω_G as follows

$$M_g \equiv \left| \frac{N_g(j\omega_g)}{D_G(j\omega_g)} \right| = \frac{1}{Q_g} \left| \frac{1}{\left(\frac{\omega_g}{\omega_G}\right)^2 + j \frac{\omega_g}{\omega_G Q_G}} \right| \tag{6o}$$

This can be approximated as

$$M_g \simeq \frac{Q_G}{Q_g} \frac{1}{\sqrt{1 + (\delta Q_G)^2}} \tag{61a}$$

in which

$$\delta = 2 \frac{\Delta\omega}{\omega_G} \simeq 2 \frac{\Delta\omega}{\omega_g} \tag{61b}$$

Likewise, we have

$$M_G \equiv \left| \frac{N_g(j\omega_G)}{D_G(j\omega_G)} \right| \simeq \frac{Q_G}{Q_g} \sqrt{1 + (\delta Q_g)^2} \tag{62}$$

For this example we have

$$M_g = 9.3 \text{ dB} \qquad M_G = 13.6 \text{ dB}$$

which is in agreement with the result in Fig. 11. These results are summarized in Fig. 12 and Table 2.

In Figs. 13a and 13b the validity of the analytical transfer function obtained in Eq. (49) is tested for cases in which the glitch occurs either near the high-frequency corner, ω_H, or near the low-frequency corner, ω_L. In Fig. 13a, all the circuit parameters were kept the same as in Fig. 11 except that the magnetizing inductance was reduced to $L_m = 1$mH in order to push the glitch near the vicinity of ω_H. It is worthwhile to note in this figure that the zero of the glitch is very well damped in comparison to Fig. 10. The reason for this is that Q_g in Eq. (47) becomes smaller because q_p and q_R in Eqs. (48c) and (48d) decrease with decreasing L_m. In Fig. 13b the glitch was pushed below the low-frequency corner by increasing the magnetizing inductance to $L_m = $ 10011111" find the duty cycle to $D = .4$. In addition, the values of the following components were modified

$$r_1 = 1\Omega \quad r_2 = 2\Omega$$
$$C_2 = 2.67\mu\text{F} \quad (C_{2s} = 50\mu\text{F})$$
$$C_o = 10.85\mu\text{F} \quad (C_{os} = 200\mu\text{F})$$

As can be seen, the analytical approximations are in good agreement with the circuit model except for the peaking at ω_H as explained earlier.

ELIMINATION OF THE GLITCH BY DAMPING THE ENERGY TRANSFER CAPACITOR

If the energy transfer capacitor C_1 is damped by an RC network as shown in Fig. 14a, then the parallel resonance in Fig. 9 discussed earlier would reduce to the one in Fig. 14b in which r_1 and r_2 have been ignored because most of the damping will now be due to r_d. Since we only intend to decrease the Q-factor from a few hundred down to the teens, the resonant frequency remains hardly changed. This implies that if the time constant $r_d C_d$ is chosen such that $r_d C_d < 1/\omega_o (\omega_o = \omega_g \sim \omega_G)$, then the Q-factor is given by

$$Q_d \simeq \frac{r_d}{\omega_o L_m} \qquad ; \qquad \omega_o = \omega_g \sim \omega_G \tag{63}$$

For the practical converter discussed here, let us choose $Q_d \sim 11$ and $1/r_d C_d \sim \omega_o/3$. With $\omega_o \sim 1245$ and $L_m = 15$mH the following values are obtained for r_d and C_d

$$r_d = 1300 \qquad C_d \sim .3\mu F \tag{64}$$

The control-to-output transfer function, with C_1 damped with the values of r_d and C_d in Eq. (64), is shown in Fig. 15 for $D ::.258$, .3, and .342. All the component values, including parasitic resistances, are the same as in the case of Fig. 10. As can be seen, the glitch has almost disappeared from the entire range. Hence, with C_1 damped, the control-to-output transfer function in Eq. (49) reduces to

$$G_d(s) \simeq K_d \frac{N_h(s)}{D_L(s)D_H(s)} \tag{65}$$

because the complex poles and zeros of the glitch essentially cancel out. The damping resistor r_d has almost no effect on the low-frequency quadratic so that $D_L(s)$, w], and Q_L are still given by Eqs. (53), (17a) and (17b) respectively. The damping resistor r_d also has no effect on the high-frequency corner so that ω_H is still given by Eq. (55). The Q-factor, Q_H in $D_H(s)$, however, is highly effected by r_d and is no longer given by Eq. (57a) or (57b). In order to determine Q_H in the presence of r_d, we need only redetermine the coefficient b_5 which according to the N-Extra Element Theorem [11] is given by

$$b_{5d} = \frac{L_2}{R}L_\sigma C_1 L_m \frac{C_2}{D'^2}\left[1 + \frac{C_o}{C_1}\frac{R}{r_d}\right] = b_5\left[1 + \frac{C_o}{C_1}\frac{R}{r_d}\right] \tag{66}$$

(In arriving at this expression, C_d is assumed to be practically a short circuit and that r_d is in parallel with C_1). Now, according to Eq. (57a), the damped Q-factor can be expressed in terms of Q_H as

$$Q_{Hd} = \frac{Q_H}{1 + \frac{C_o}{C_1}\frac{R}{r_d}} \tag{67}$$

in which Q_H is given in Eq. (57a) or (57b). The high frequency quadratic is now given by

$$D_H(s) = 1 + s/Q_{Hd}\omega_H + (s/\omega_H)^2 \tag{68}$$

in which, as mentioned earlier, ω_H is still given by Eq. (55).

The damped control-to-output transfer function in Eq. (65) is compared with that of the circuit model for $D = .342$ in Fig. 16. The agreement between the analytical approximation and that of the actual circuit model is seen to be very good.

CONCLUSIONS

A detailed analysis of the isolated Ćuk converter has shown that a very good method to eliminate the glitch in the control-to-output transfer function is to choose the ratio of the capacitances of the two energy capacitors according to the condition derived in Eq. (32) and to lightly damp one of the two capacitors. Using this method, the isolation transformer can be designed without the additional constraint of having to have a large (or very small) magnetizing inductance.

APPENDIX

Figure 17 shows control-to-output transfer function when the magnetizing inductance is reduced to $l_m = .4$mH and the following values are used

$$D = .42, \quad C_2 = .229\mu\text{F} \ (C_{2s} = 4.3\mu\text{F}), \quad C_1 = 2.5\mu\text{F} \ (C_{1s} = 47\mu\text{F})$$

The remaining values, including the parasitic elements, are the same as before. For this converter, such a small value of l_m is not practical at all because the high input voltage will cause large swings in the flux density in a core of reasonable size. Hence, this example will be used only for purposes of numerical illustrations and not as a practical design.

In Fig. 7, the peaking in the high-frequency response is due to the two pairs of complex poles ω_H and ω_G while the notch due to the zero of the glitch is well damped as in Fig. 3a. The approximate expressions derived earlier in general will not hold because those expressions were derived under the assumption that $\omega_G < \omega_H$ and not $\omega_G > \omega_H$. Since we now have $\omega_L < \omega_H < \omega_G$, is possible to factor the denominator approximately as

$$D(s) \simeq D_0(s)\left(1 + \frac{b_3}{b_2}s + \frac{b_4}{b_2}s^2\right)\left(1 + \frac{b_5}{b_4}s + \frac{b_6}{b_4}s^2\right) \tag{a.1}$$

and find

$$D_H(s) = 1 + \frac{b_3}{b_2}s + \frac{b_4}{b_2}s^2 = 1 + s/Q_H\omega_H + (s/\omega_H)^2 \tag{a.2}$$

$$D_G(s) = 1 + \frac{b_5}{b_4}s + \frac{b_6}{b_4}s^2 = 1 + s/Q_G\omega_G + (s/\omega_G)^2 \tag{a.3}$$

It follows from these equations that

$$\omega_H = \sqrt{\frac{b_2}{b_4}} \qquad Q_H = \frac{b_2}{b_3\omega_H} \tag{a.4}$$

$$\omega_G = \sqrt{\frac{b_4}{b_6}} \qquad Q_G = \frac{b_4}{b_5\omega_G} \tag{a.5}$$

A though the preceding development is acceptable, a somewhat more interest ng approach will be given next.

It was shown earlier in Eq. (18a) that the high-frequency corner in the limit $L_m \to \infty$ is given by

$$\omega_H' = \sqrt{\frac{L_1}{L_2 L_\sigma C_o} + \frac{L_\epsilon}{L_2 L_\sigma}\frac{D'^2}{C_1 \| C_2}} \tag{a.(i)}$$

Next, the high-frequency corner n the imit $L_m \to 0$ is obtained from b_i in Eqs. (10a-d)

$$\omega_H'' \approx \lim_{L_m \to 0}\sqrt{\frac{b_2}{b_4}} = \sqrt{\frac{L_1}{L_\sigma L_2 C_o} + \frac{L_\epsilon}{L_\sigma L_2 C_\epsilon}} \tag{a.7}$$

If we now **require** that the removal and zero-ripple coupling conditions in Eq. (33) be satisfied, i.e., $C_2/C_1 = D'/D$ and $\alpha = 1$, then we get

$$\frac{C_1 \| C_2}{D'^2} = C_\epsilon = \frac{C_1}{D'} \tag{a.8}$$

which implies that $\omega_H' = \omega_H'' = \omega_H$. Hence, we conclude that, with the removal condition satisfied, ω_G must still be given as before since W_H remains unchanged in the extreme limits of L_m. Furthermore, Q_g will now be considerably higher because, with $C_2/C_1 - \alpha D'/D \to 0$, $q_R \to \infty$ as can be seen in Eq. (48d). It follows that the removal condition derived earlier is still effective for very small values of L_m so that if we now choose

$$C_2 = C_1\frac{D'}{D} \Rightarrow C_2 = .4557)\ 11'\ (C_{2s} = 8.557\mu F)$$

the peaking at ω_G must substantially diminish. This is verified in Fig. 18. Any slight deviation from the removal condition, will cause Q_g to decrease drastically allowing for the high-Q pole of the glitch to

show up without the benefit of a very closely spaced high-Q zero to counter its peaking. In what follows, the approximate control-to-output transfer function will be determined for $\omega_G > \omega_H$.

In the approximate control-to-output transfer in Eq. (50), Q_g, ω_G and ω_H must now be redetermined for $\omega_G > \omega_H$. All other parameters remain essentially the same. In Eq. (47), Q_g was derived assuming that the dominant term in a_2 was $L_m(C_1 + C_2)$. Since L_m is small now, that assumption is not valid except when $\alpha = 1$ and $C_2 - C_2 \alpha D/D' = 0$. In this case, according to Eq. (45) we have

$$Q_g = \frac{1}{\omega_g a_1 - \frac{\omega_g}{\omega_h} \frac{1}{Q_h}}$$
(a.9)

in which Q_h is given by Eq. (49). This can be written as

$$Q_g = q_1 \parallel q_2 \parallel q'_R \parallel q_g$$
(a.10)

in which q_1 and q_2 are given, as before, by Eqs. (48a) (48b) respectively and q_g and q'_R are given by

$$q_g = Q_h \frac{\omega_h}{\omega_g} = Q_h \big|_{\omega_h = \omega_g}$$
(a.11)

$$q'_R = \frac{R}{\omega_g L_1 \left(\alpha + \frac{D}{D'}\right) \frac{D}{D'}}$$
(a.12)

The high-frequency corner ω_H for small L_m is nearly independent of L_m and is now given by

$$\omega_H = \omega''_H = \sqrt{\frac{L_1}{L_\sigma L_2 C_o} + \frac{L_e}{L_\sigma L_2 C_e}}$$
(a.13)

so that ω_G is obtained from

$$\omega_G = \frac{1}{\omega_H \omega_L \sqrt{b_6}}$$
(a.14)

Performing the necessary substitution we get

$$\omega_G = \frac{1}{\sqrt{L_m(C_1 + C_2)}} \sqrt{\frac{1 + \frac{L_e C_o}{L_1 C_e} \frac{C_e}{C_1 \parallel C_2} D'^2}{1 + \frac{L_e C_o}{L_1 C_e}}} \simeq \frac{1}{\sqrt{L_m(C_1 + C_2)}}$$
(ii. JF))

Since ω_G is still approximately given by the parallel resonance of L_m and ("1 + C_2 in Fig. 9, Q_G is still given by Eq. (39) as before. Since ω_G, ω_H, and Q_G are all still given approximately as before, it follows that Q_H is still approximately the same as before because from the high-frequency behavior of $D(s)$ we have

$$\frac{b_5}{b_2} \simeq \frac{1}{\omega_G^2} \frac{1}{\omega_H Q_H} + \frac{1}{\omega_H^2} \frac{1}{\omega_G Q_G}$$ (ii.1(i))

Since all quantities in Eq. (a.16) except for Q_H remain unchanged, it follows that Q_H remains essentially unchanged. In Figs. 17 and 18 the dotted lines are the approximate transfer functions which are in very good agreement with the circuit, model.

Figure 19 shows how the magnitude response changes as the duty-cycle is decreased from $D = .42$ in Fig. 18 to $D = .35$. In the same figure, the phase response snows excessive phse shift because of the complex right-half plane zero at $f = 7.5$kHz. It is possible to improve the phase repsonse by damping C_1 as before and setting the time constant $r_d C_d \simeq 1/\omega_G$ so that

$$r_d = 300\Omega \text{ and } C_d = 1\mu F$$

The damped response is shown in Fig. 20

REFERENCES

[1]   S. Krauthamer, R. Das, V. Vorperian, J. White, J. Bennett and D. Rogers, "High-Effic iency Synchronous Rectification in Spacecraft Power Systei ns," Proceedings of tile European Space Power Conference, Graz, Austria, August 23-27, 1993, pp. 179-183.

[2]   W. Polivka 1'. Chetty and R. Middlebrook, "State-Space Average Modeling of Converters with Parasitic and Storage-Time **Modulation**," Proceedings of the 1980, IEEE Power Electronics Specialist Conference, Record PESC'80.

[3]   R.D. Middlebrook, "Low-Entropy Expressions: The Key t o Design-Oriented Analysis," Proceedings of the IEEE Frontiers in Education, 21st Annual Conference, Purdue University, September 21-24, 1991; 399-403

[4]   W. Behen, "Analysis of the Effect of the Magnetizing Inductance in an Isolated Cuk Converter," Technical Notes **of** the Caltech Power Electronics Group, '1%5, Nov. **1979.**

[5]   S. Cuk and L. Kajouke, "Electric and Magnetic Circuit Interactions in Switching Converters," Proceedings of the IEEE Applied Power Electronics Conference, March 2-6, 1987, San Diego, CA.

[(i] V. Vorpérian, "Sirn plified Analysis of PWM Converters Using the Model of the PWM Switch, Part 1, Continuous Conduction Mode," IEEE Transactions on Aerospace and Electronics Systems, V()] 26, No. 2, May 1990, pp. 490-496

['1] V. Vorpérian, "Simplified Analysis o f PWM Converters Using the Model of the PWM Switch, Part II, Discontinuous Conduct ion Mode," IEEE Transactions on A erospace and Electronics Systems, Vol 26, No. 2, May 1990, pp. 497-5 05.

[8] V. Vorpérian, "Analysis of Current-Mode Controlled Converters Using the Model of t he C ~urrctlt-Cont rolled PWM Switch," Proceedings of the PCIM'90 Conference, October 23-25, Philadelphia, 1'A, pp.183-195.

[9] The Design Center, User's Guide, Microsim Corporation.

[10] R.D. Middlebrook, "N ull Double Injection and the Extra Element Theorem," IEEE Transactions on Education, Vol. 32, No. 3, August 1989, pp.167-180.

[1 1] R.D. Middlebrook, "The Two Extra-Element Theorem, " Proceedings of the IEEE Frontiers in Education, 21st Annual Conference, Purdue University, September 21-24, 1991; 399-403
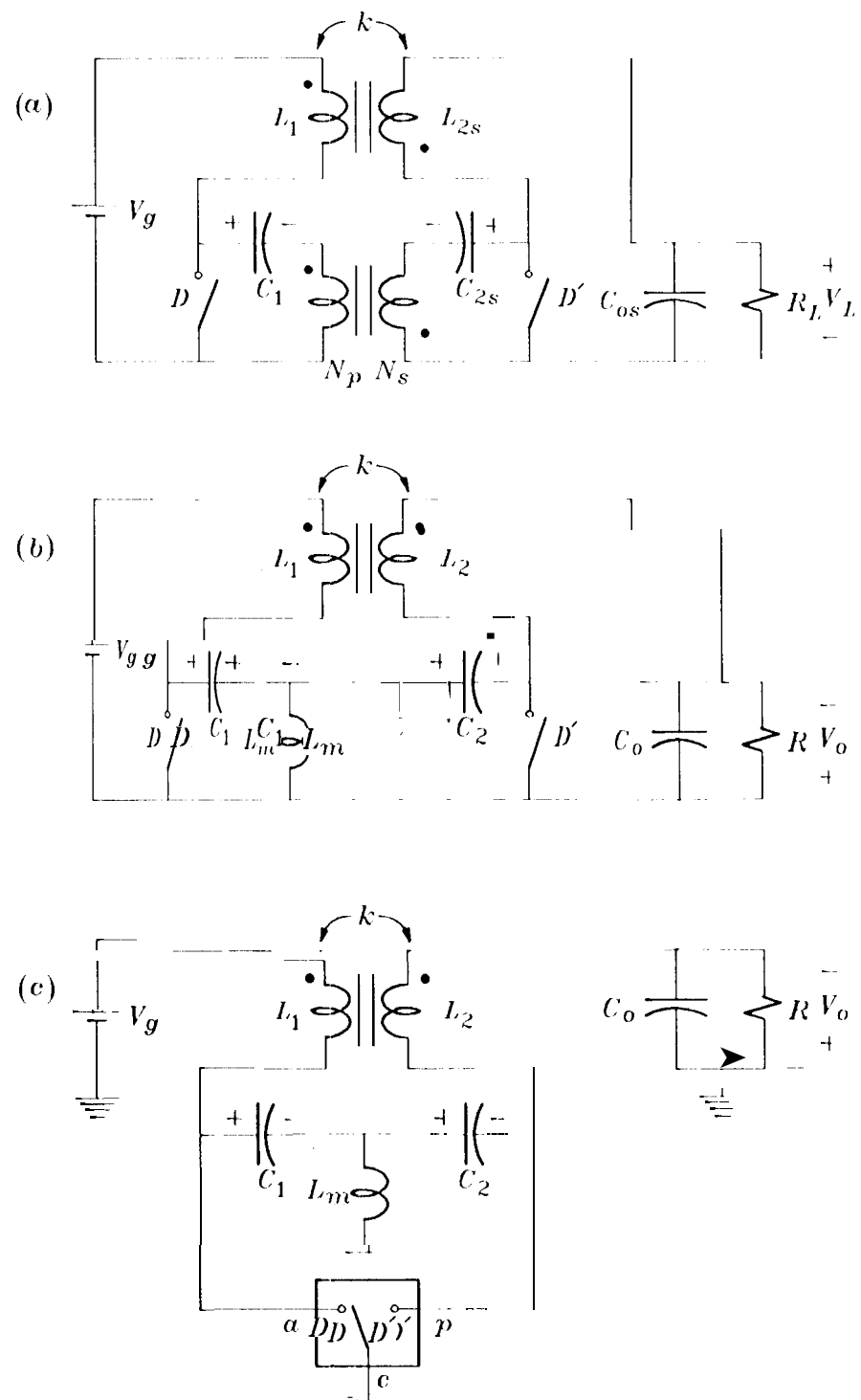
Fig. 1   a) The isolated Cuk converter with coupled input and output inductors. b) Reflection of the secondary components to the primary. c) Identification of the PWM switch.
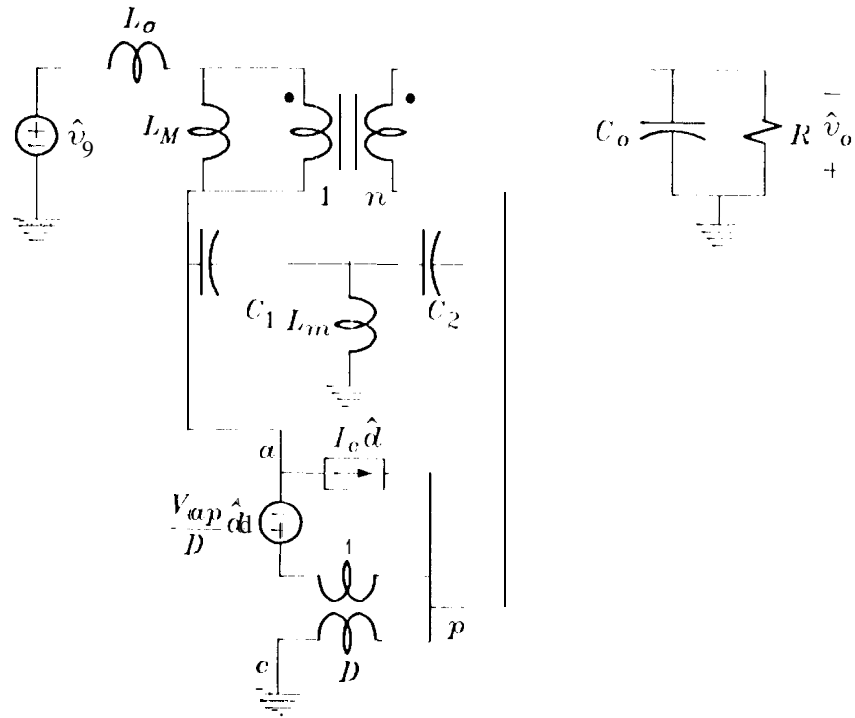
Fig.2 The complete small-signal equivalent circuit model of the Cuk converter obtain by replacing the PWM switch with its equivalent circuit model in continuous conduction mode.

([1])

(b)
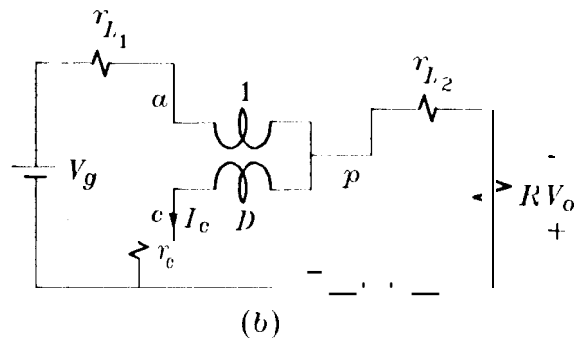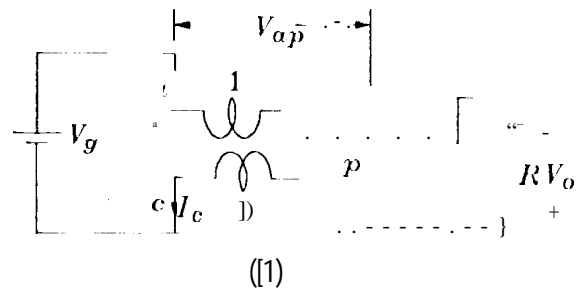
Fig 3. Equivalent circuit model for dc analysis a) without parasitic elements and b) with parasitic elements

Fig. 4 a) The equivalent circuit model for the determination of the control-to-output transfer function. b) The equivalent circuit model in a) under the null condition in $\hat{i}_{L_2}(s)$.
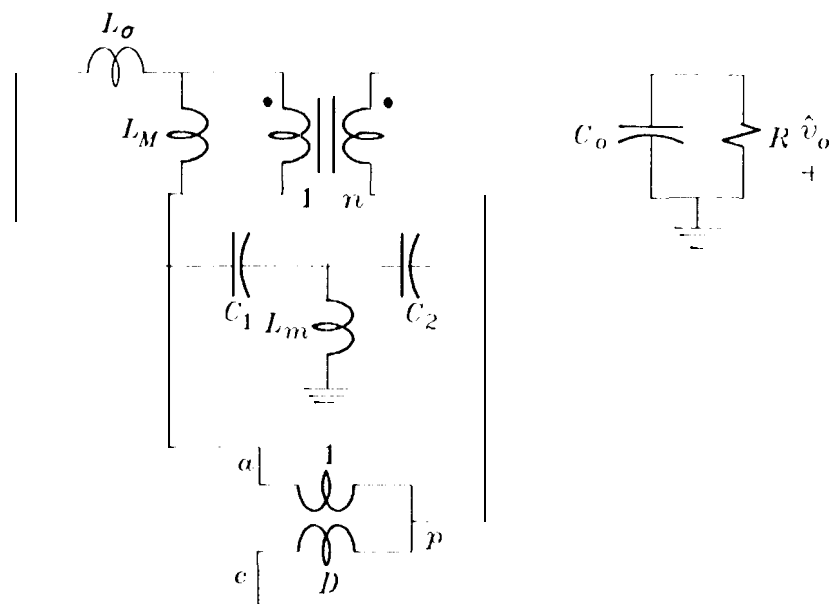
Fig. 5 The equivalent circuit model for the determination of $D(s)$.

<div align="center">

Table 1

$L_1 = 2.5\text{mH}$	$C_1 = .33\mu\text{F}$	$L_m = 151111[$
$L_2 = .66\text{mH}$	$C_{2s} = 66\mu\text{F}$	$N = 4.333$
$k = .449$	$C_{os} = 470/11"$	$R_L = 15\Omega$
$V_g = 270\text{V}$	$F_s = 30\text{kHz}$	$D = .3$

</div>
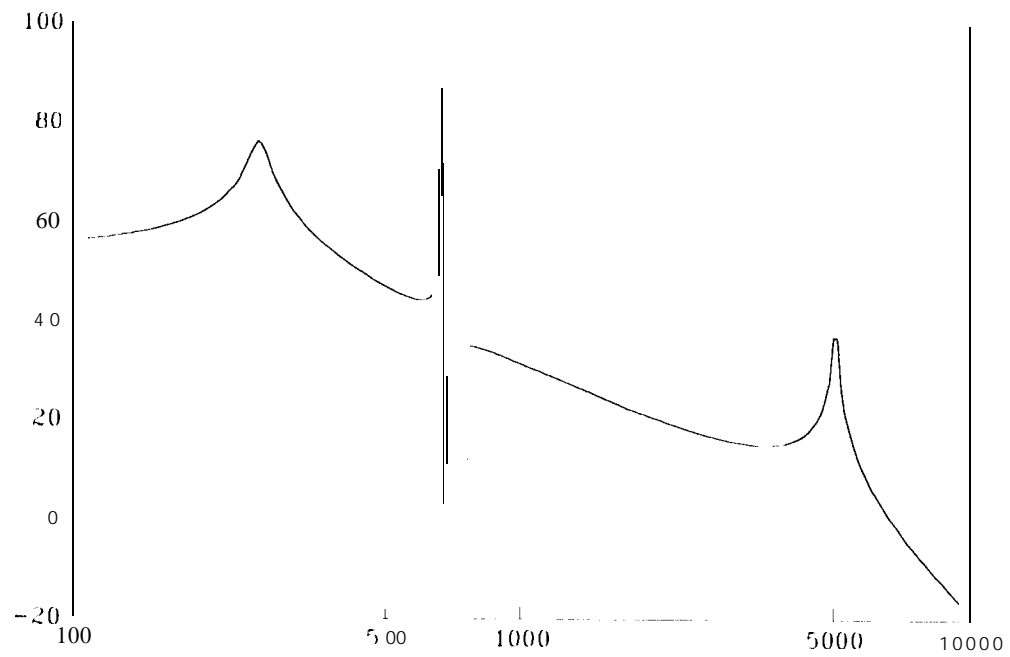
Fig. 6 The control-to-output transfer function of the Cuk converter with elements shown in Table I
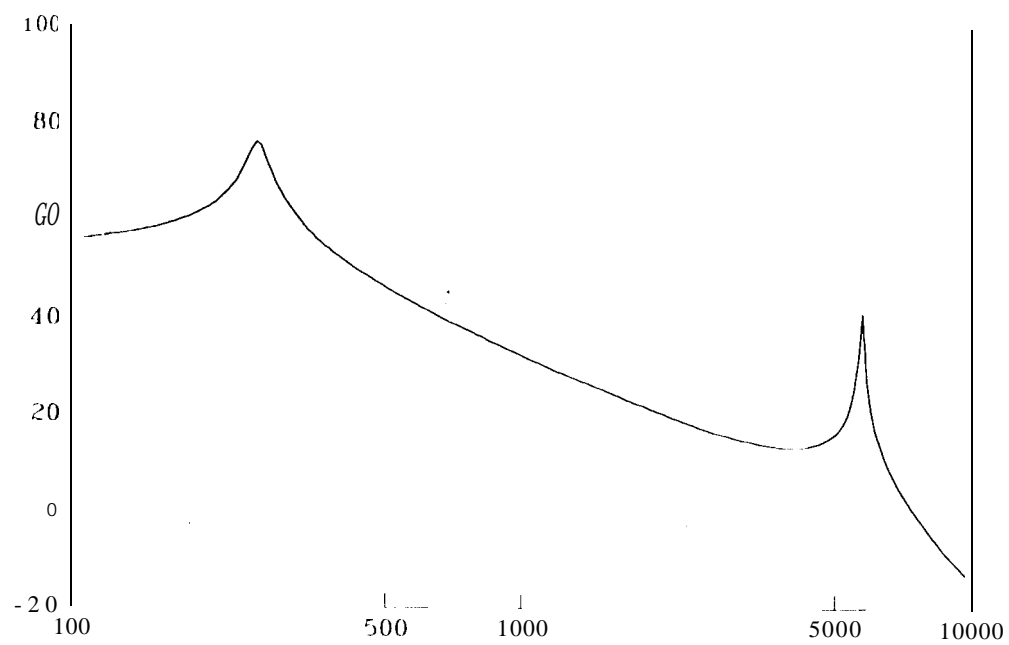
Fig. 7 Elimination of the glitch from the control-to-output transfer function in Fig. 6 by satisfying the removal condition in Eq. (32).
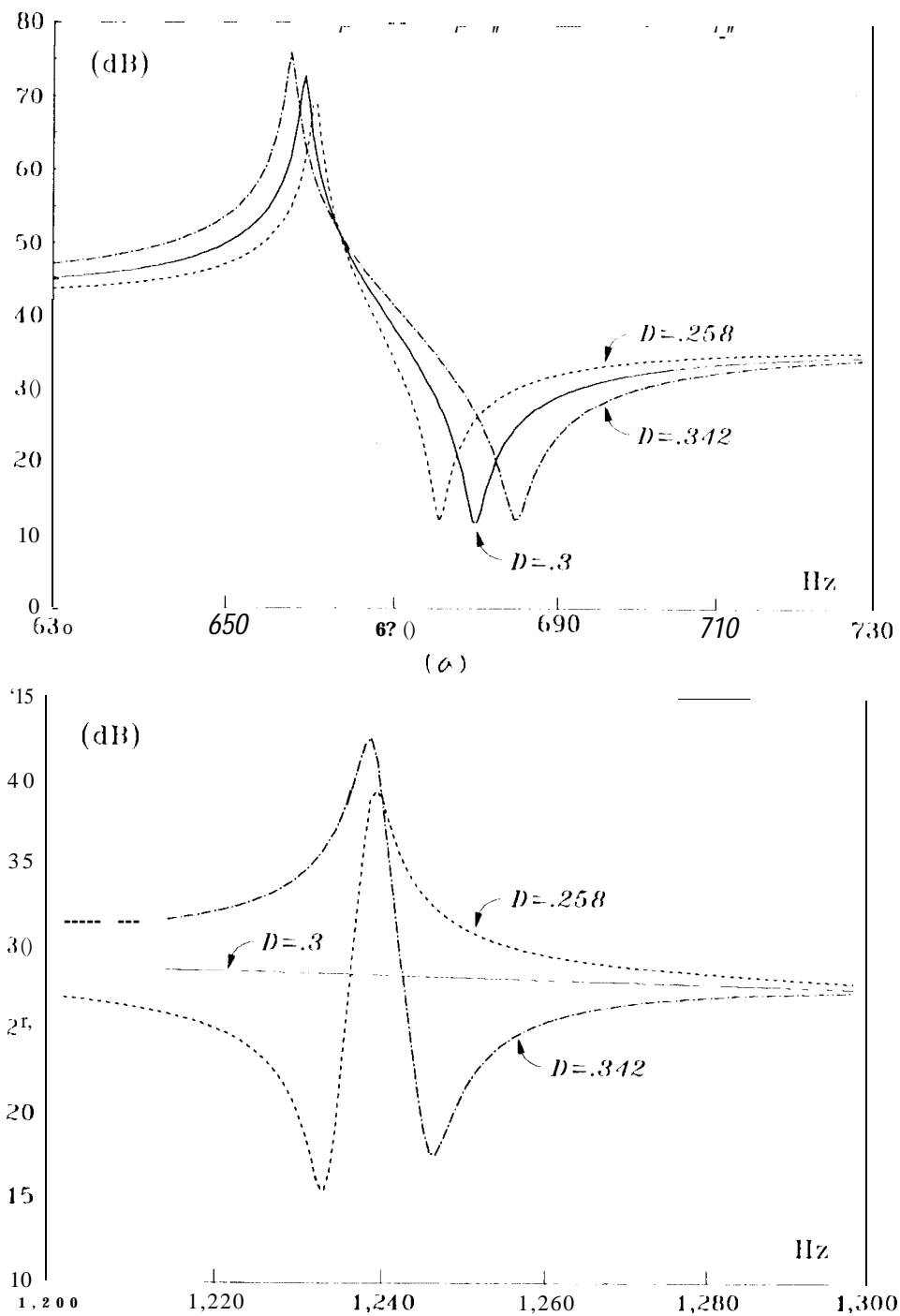
Fig. 8 a) The behavior of the glitch for .258 < f) < .342 without satisfying the removal condition and b) with the removal condition satisfied at $D = .3$.
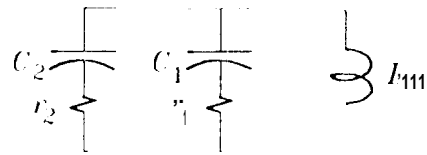
Fig. 9 The equivalent circuit model for the determination of he damping of he complex poles of the glitch.
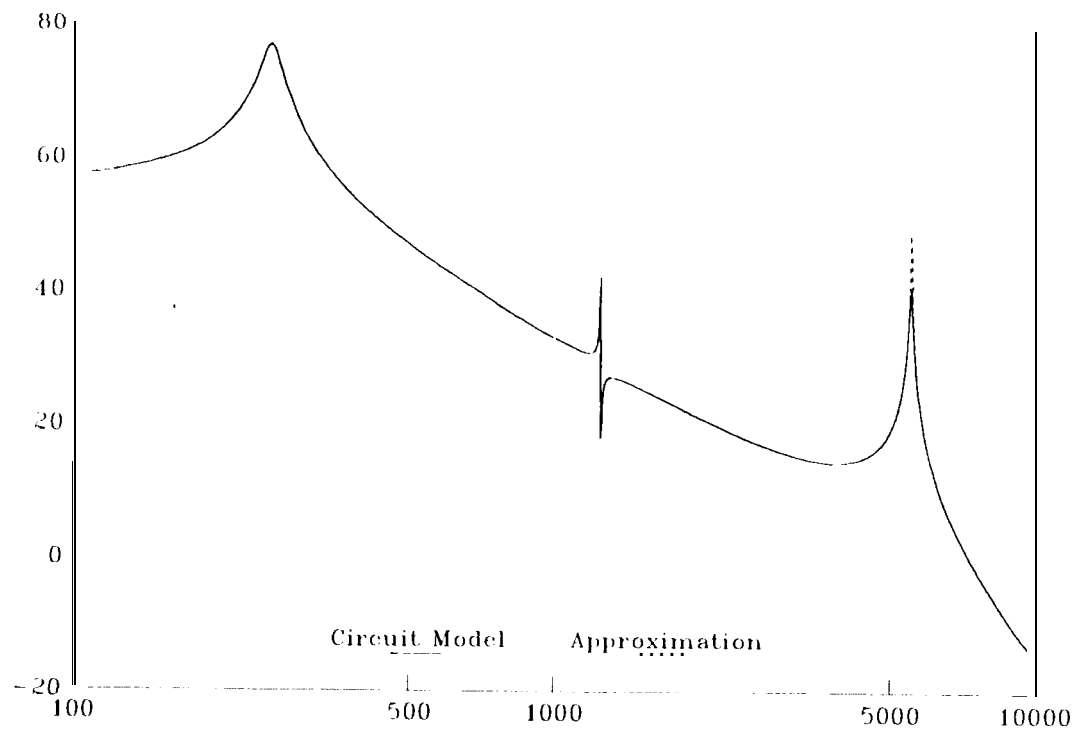
Fig. 10 The control-to-output transfer function for $D = .342$ in the presence of parasitic elements for 1) $= .342$ with removal the removal condition satisfied at $D = .3$.
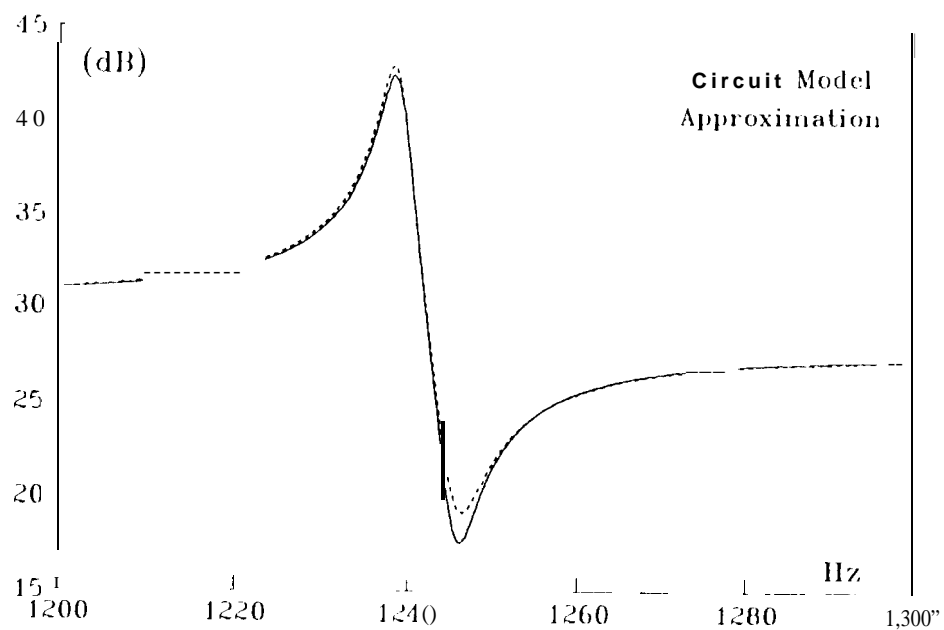
Fog. 11 Comparison of the approximate transfer function with the circuit model around the glitch in Fig. 10.
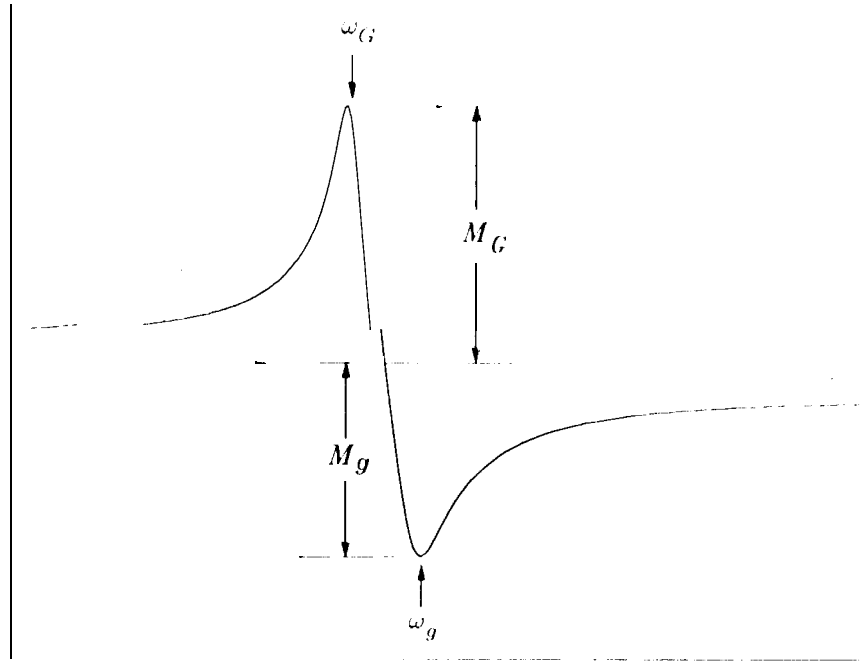
Fig. 12 Definitions M_G and M_g in the glitch.

TABLE 2

$$\omega_g = \frac{1}{\sqrt{L_1\left(C_1 - \alpha C_2\frac{D}{D'}\right) + L_m(C_1 + C_2)}}$$

$$\omega_G = \frac{1}{\sqrt{L_1\left(C_c - \frac{C_1 \| C_2}{D'^2}\right) + L_m(C_1 + C_2)}}$$

$$Q_G = Q_1 \| Q_2 \| Q_c$$

$$Q_g = q_1 \| q_2 \| q_p \| q_R$$

$$Q_1 = \frac{1}{\omega_G C_1 r_1}$$

$$q_1 = \frac{1}{\omega_g C_1 (r_1 + r_{L_1})}$$

$$Q_2 = \frac{1}{\omega_G C_2 r_2}$$

$$q_2 = \frac{1}{\omega_g C_2 r_2}$$

$$Q_c = \omega_G C_1 \| \frac{1}{C_2(r_1 + r_2)}$$

$$q_p = \frac{-1}{\omega_g C_1 \| C_2\left[r_2(1 + \frac{L_1}{L_m}) + r_1(1 - \alpha\frac{D}{D'}) + r_{L_1}\right]}$$

$$q_R = -\frac{R}{\omega_g L_1}\frac{L_m}{L_1 C_1}\frac{C_1 + C_2}{C_1 - C_2\alpha D/D'}$$

$$M_g \simeq \frac{Q_G}{Q_g}\frac{1}{\sqrt{1 + (\delta Q_G)^2}}$$

$$M_G \simeq \frac{Q_G}{Q_g}\sqrt{1 + (\delta Q_g)^2}$$
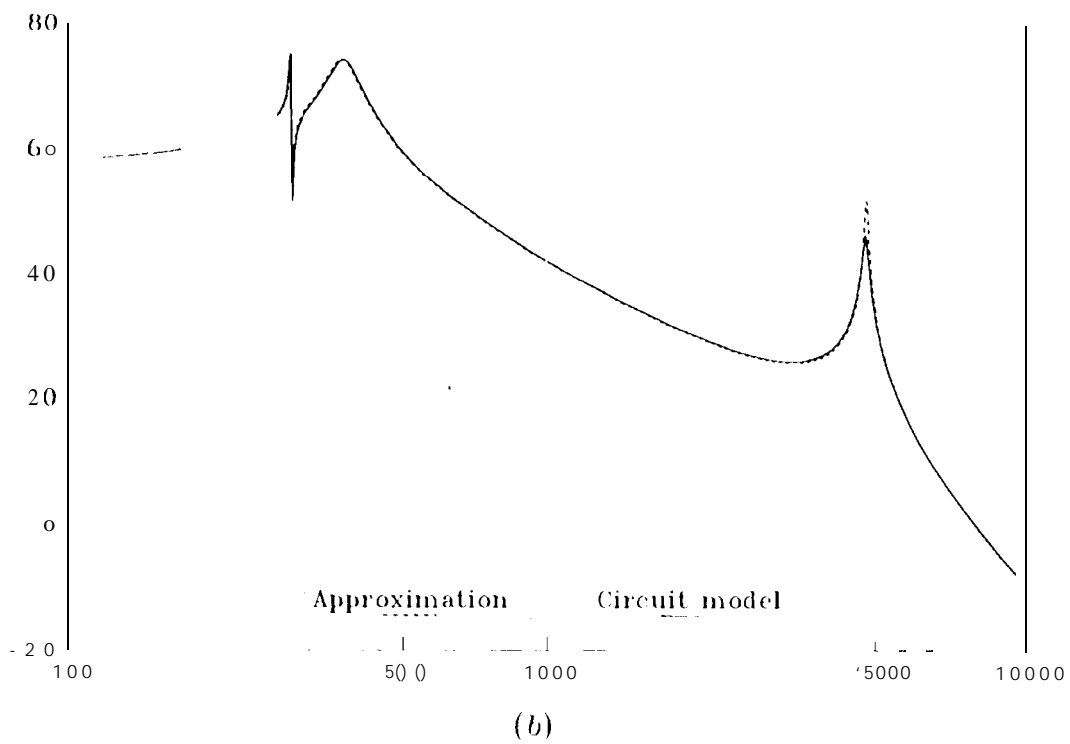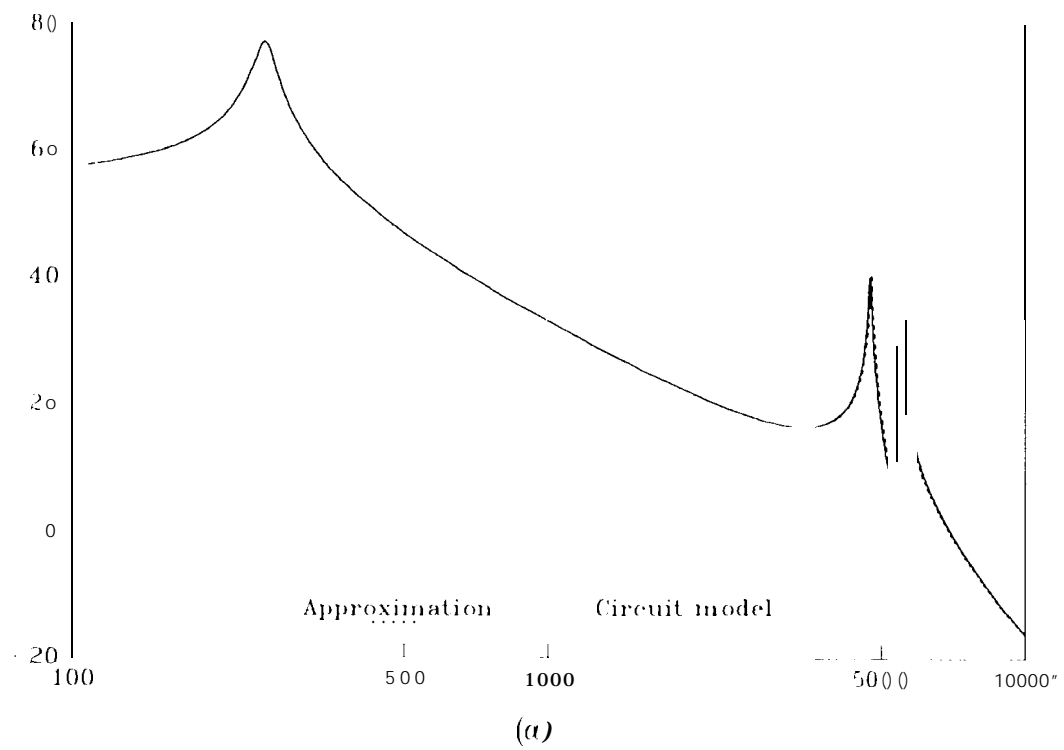
Fig. 13 a) Comparison of the approximate transfer function with the circuit model when the glitch is pushed near ω_H and b) near ω_L.
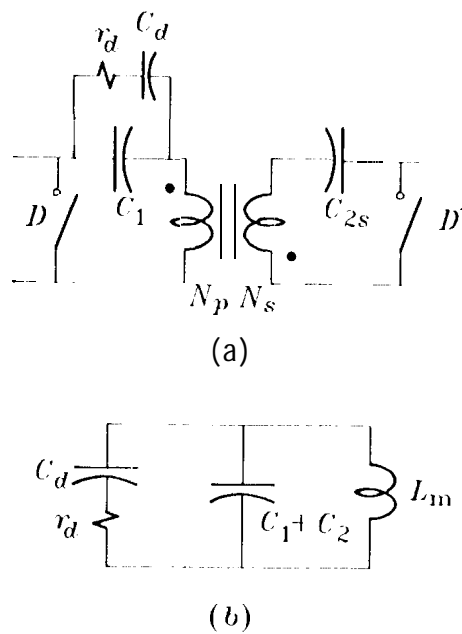
(a)

(b)

Fig. 14 a) Damping of the energy transfer capacitor C_1. b) The equivalent circuit model for the determination of the damping of the high-frequency quadratic $D_{II}(s)$.
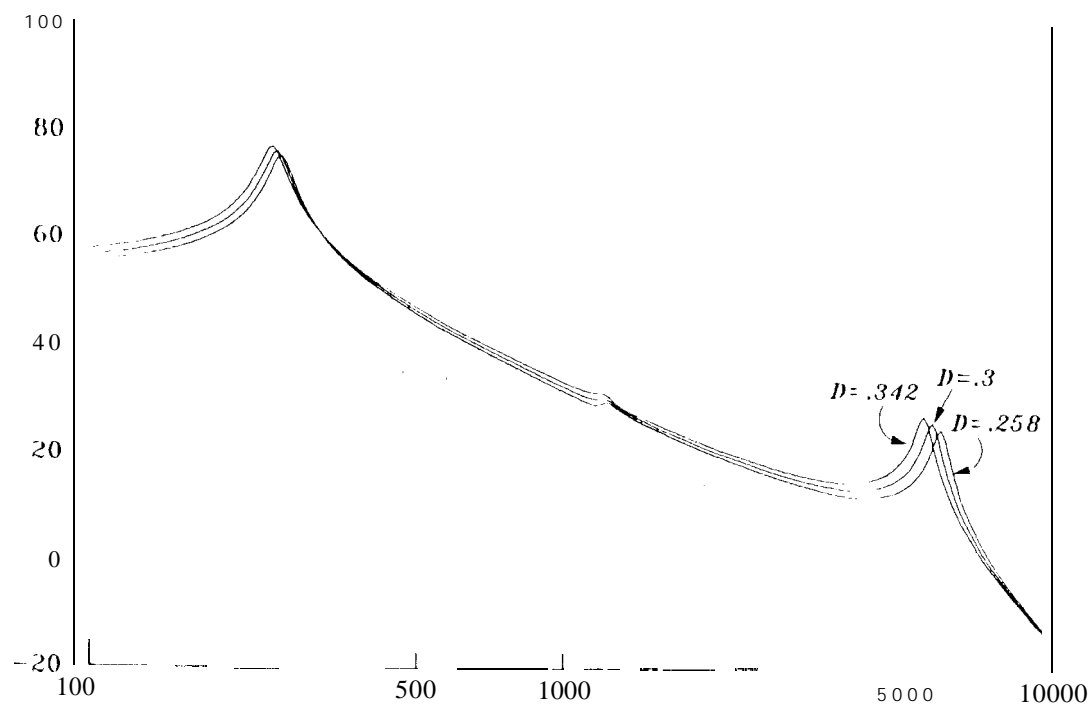

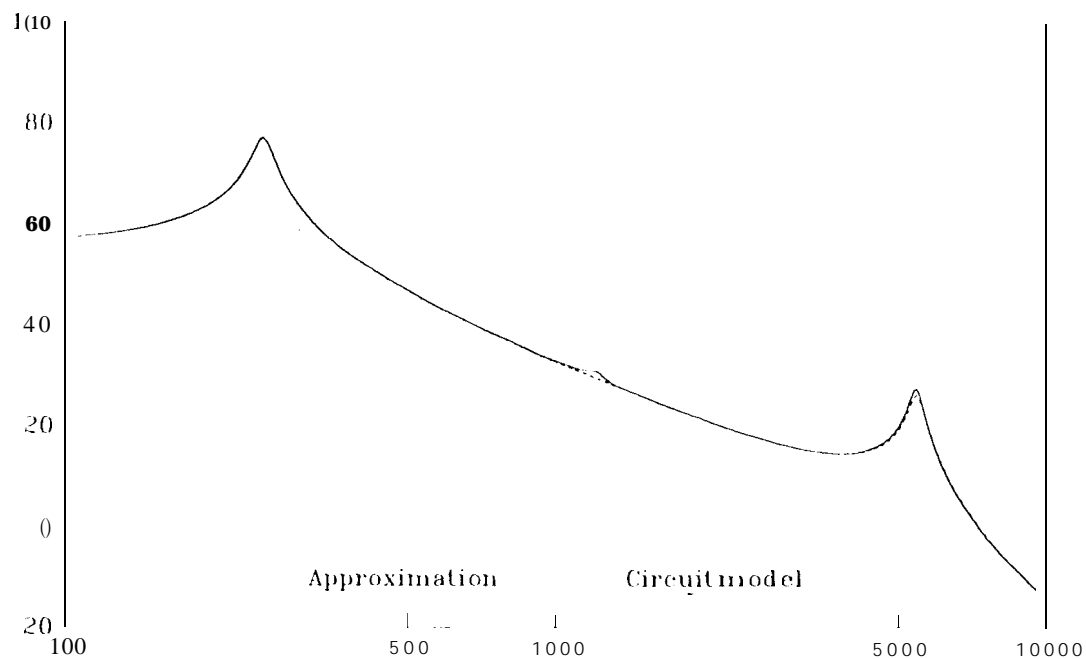**Fig. 15** The damped response for $.258 < D < .342$ for a choice of $C_d = .3\mu F$ and $r_d = 1300\Omega$

Fig. 16 Comparison of the approximate damped ansfer function with the circuit model for $D = .342$.
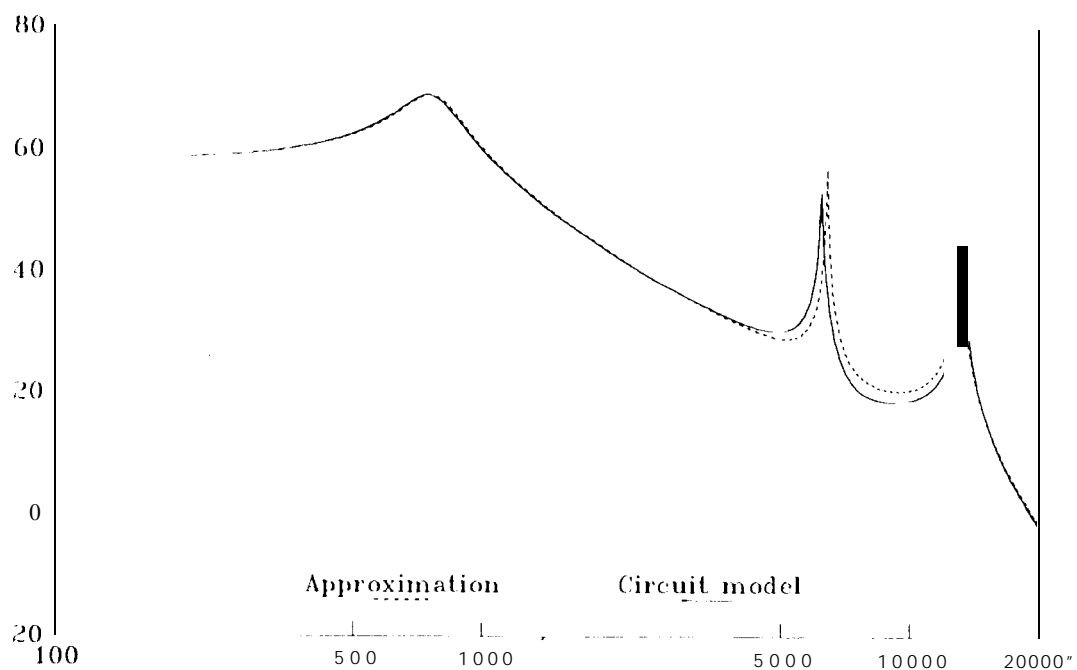
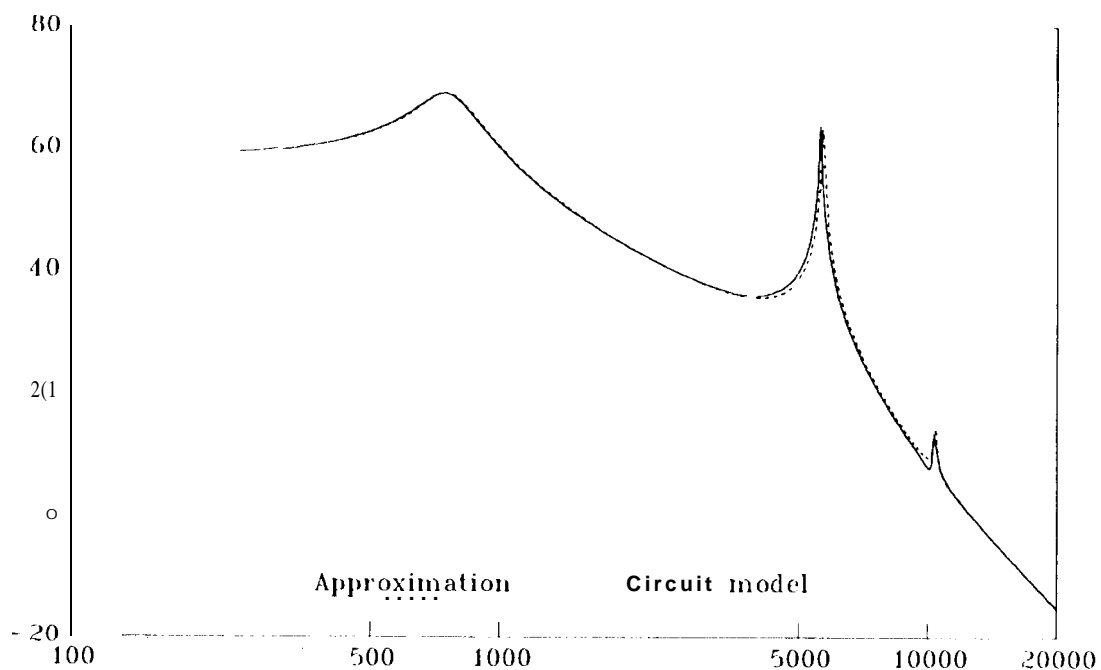**Fig. 7** The control-to-output transfer function when $\omega_G > \omega_H$.

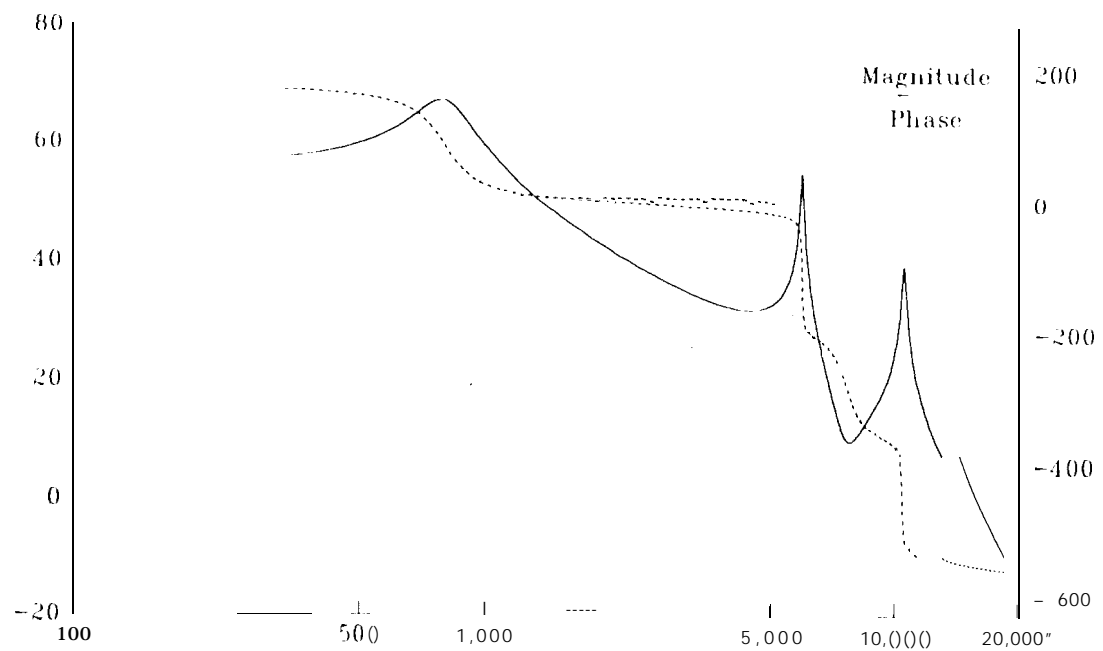**Fig. 18** The control-to-output transfer function with the removal condition satisfied

Fig. 19 The undamped control-to-output transfer function as the duty-cycle changes from D = .42 in Fig. 18 to D = .35
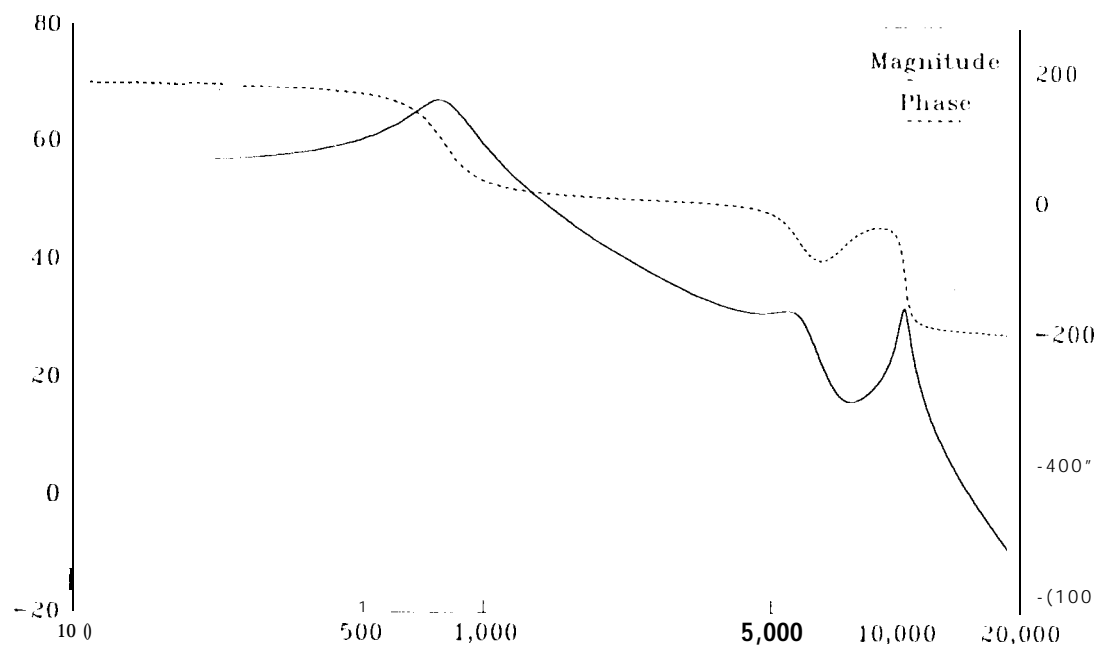

Fig. 20 The damped control-to-output transfer function.